New Journal of Physics
The open access journal at the forefront of physics

Deutsche Physikalische Gesellschaft DPG
IOP Institute of Physics

Published in partnership with: Deutsche Physikalische Gesellschaft and the Institute of Physics

OPEN ACCESS

RECEIVED
14 March 2018

REVISED
31 May 2018

ACCEPTED FOR PUBLICATION
26 June 2018

PUBLISHED
6 July 2018

PAPER

Multiphoton nonclassical light from clusters of single-photon emitters

Luo Qi[1,2], Mathieu Manceau[1], Andrea Cavanna[1,2], Fabian Gumpert[1,2], Luigi Carbone[3], Massimo de Vittorio[4], Alberto Bramati[5], Elisabeth Giacobino[5], Lukas Lachman[6], Radim Filip[6] and Maria Chekhova[1,2]

[1] Max-Planck-Institute for the Science of Light, Erlangen, Germany
[2] University of Erlangen-Nürnberg, Staudtstrasse 7/B2, D-91058 Erlangen, Germany
[3] CNR NANOTEC-Institute of Nanotechnology c/o Campus Ecotekne, University of Salento, via Monteroni, Lecce, I-73100, Italy
[4] Center for Biomolecular Nanotechnologies, Istituto Italiano di Tecnologia, Via Barsanti 14, I-73010 Arnesano, Lecce, Italy
[5] Laboratoire Kastler Brossel, UPMC-Sorbonne Universits, CNRS, ENS-PSL Research University, College de France, France
[6] Department of Optics, Palacky University, 17 Listopadu 12, Olomouc 77146, Czechia

E-mail: maria.chekhova@mpl.mpg.de

Keywords: single-photon emitters, multiphoton nonclassical light, antibunching, colloidal quantum dots

Abstract

We study nonclassical features of multiphoton light emitted by clusters of single-photon emitters. As signatures of nonclassicality, we use violation of inequalities for normalized correlation functions of different orders or the probabilities of multiphoton detection. In particular, for clusters of 2–14 colloidal CdSe/CdS dot-in-rods we observe antibunching and nonclassicality of up to the fourth-order. Surprisingly, violation of certain classical inequalities gets even more pronounced for larger clusters.

1. Introduction

The development of quantum technologies requires advanced sources of nonclassical light. In particular, there is a challenge to go beyond single-photon states, two-photon states, and squeezed states, available at the moment. One way is nonlinear optical interactions of higher orders, leading to the emission of photon triplets, quadruples and so on [1]. Realization of such processes remains a challenge, although there are several experimental attempts to generate photon triplets through the third-order interaction in nonlinear crystals [2], waveguides [3], and fibers [4]. Generation of photon triplets from solid-state emitters, such as 'quantum dot molecules' [5] is another option. Finally, multiphoton states can be produced by heralding and interference applied to sufficiently bright twin beams, obtained through high-gain parametric down-conversion. Recent experimental achievements include demonstration of 10-photon entanglement [6] and up to 50-photon nonclassical states [7].

Here we consider a much simpler method, which is to combine single-photon emitters into a group (a cluster) and obtain light with a limited number of photons [8]. For such a cluster, the number of photons will not significantly exceed the number of emitters, which suggests applications in quantum key distribution (QKD) [9] and quantum metrology [10], where a limit on the maximal number of the photons is highly relevant. Recently, it has been predicted that even a large number of realistic single-photon emitters can produce nonclassical light [8, 11]. Importantly, this way of obtaining multiphoton quantum states does not require postselection or heralding, unlike methods based on nonlinear optical effects.

The focus of this work is on the quantum properties of light emitted by clusters of colloidal quantum dots. By independently estimating the number of emitters in a cluster, we study the nonclassical features as functions of this number. Using different nonclassicality criteria, we see that all of them are satisfied for clusters of up to 14 emitters, and some of them become even more pronounced as the number of emitters grows.

The next section introduces different nonclassicality criteria used in this paper. They are formulated in terms of correlation functions (CFs) of order higher than two as well as in terms of the probabilities of multiphoton detection. Section 3 describes the experiment on testing these criteria for clusters of semiconductor colloidal

nanocrystals. The results are presented and discussed in section 4. Section 5 is the Conclusion. Some important but bulky calculations are moved into two Appendices.

2. Witnessing nonclassicality

By definition, a nonclassical state is the one whose Glauber–Sudarshan (P) function is negative or singular [12, 13]. However, because the P function is not directly measurable in experiment, various observable sufficient conditions of nonclassicality have been formulated. Putting aside loss-sensitive features, like squeezing or Wigner function negativity, here we will focus on those accessible through direct detection with a limited efficiency.

The simplest of them is antibunching, formulated in terms of the second-order normalized CF $g^{(2)}$,

$$g^{(2)} < 1. \tag{1}$$

Sometimes its analogs involving CFs of higher orders,

$$g^{(k)} < 1, \quad k > 2 \tag{2}$$

are referred to as 'higher-order antibunching' [14]. Third-order antibunching has been observed in [14, 15] for a single quantum dot coupled to a cavity.

More general inequalities indicating nonclassicality in terms of normalized CFs of different orders have been formulated by Klyshko [13]:

$$g^{(k-1)}g^{(k+1)} < [g^{(k)}]^2. \tag{3}$$

At $k = 1$, equation (3) becomes the antibunching condition (1) because $g^{(0)} = g^{(1)} = 1$. Accordingly, one can introduce a *nonclassicality parameter of order* $k + 1$, NP$(k + 1)$, corresponding to the order of the highest CF it involves,

$$\mathrm{NP}(k + 1) \equiv g^{(k-1)}g^{(k+1)} - [g^{(k)}]^2. \tag{4}$$

Its negativity is an operational witness of nonclassicality [13]. More insight is given by plotting $g^{(k)}(k)$ in the logarithmic scale: inequality (3) means that the dependence is, around some k, convex [13]. This is an approximation of the 'extreme' case where $g^{(k)}$ drops to zero at some k, which means that there is a limited number of photons emitted. This 'drop' of normalized CFs starting from a certain value brings certain advantages in QKD and metrology, as we discuss later.

We would like to stress that conditions (3) are stronger than 'higher-order antibunching' (2) in the sense that from all conditions (3) up to $k + 1$ satisfied, all conditions (2) up to $k + 1$ follow. For instance, $g^{(2)} < 1$ in combination with NP$(3) < 0$ leads to $g^{(3)} < 1$. To the best of our knowledge, these conditions have not yet been tested in experiment.

Recently, alternative hierarchies of kth-order nonclassicality witnesses have been formulated, based on the 'click' statistics of on-off detectors [16–18]. Compared to the conditions on the 'click' statistics, an advantage of conditions (3) is that they are formulated in terms of normalized CFs, which are invariant to optical losses or detection inefficiency [13]. On the other hand, witnesses of nonclassicality [17] or quantum nonGaussianity [11] formulated in terms of multiphoton detection probabilities are more robust to noise than (3) [19].

In particular, the nonclassicality witnesses introduced in [18] are $\theta^{(k)} < 1$, where

$$\theta^{(k)} = \frac{P_{0^{\otimes k}}}{\prod_{i=1}^{k} P_{0[i]}}, \tag{5}$$

$P_{0^{\otimes k}}$ is the probability that neither of k detectors 'clicks', and $P_{0[i]}$ is the probability that the ith detector does not 'click'. They have been applied to observe the nonclassical features of emission from ensembles of color centers in diamond [19] and ions in a trap [20]. However, the nonclassicality has been witnessed only for the case of $k = 2$. In what follows, for the first time we test conditions (3) and (5) with $k = 2, 3, 4$ for clusters of up to 14 emitters.

3. Experiment

In our experiment we use colloidal semiconductor quantum dots [21]. These emitters, although featuring a certain amount of blinking [22] and bleaching [23], and a non-negligible probability of two-photon emission, are very convenient due to their room-temperature operation and relatively simple production. The 'dot-in-rod' (DR) modification [24] is especially promising because of reduced blinking and a high degree of polarization [25–27]. Clusters are easily formed [8, 28] by dropping a DR solution onto a substrate and leaving the solvent to evaporate, the mean number of DRs in a cluster depending on the solution concentration. For this work we use

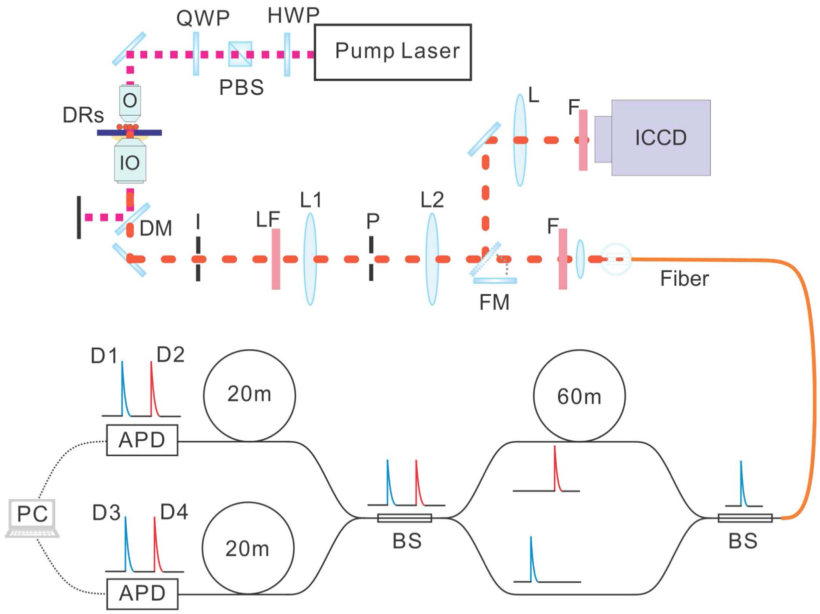

Figure 1. The experimental setup. DR clusters are excited by the 3rd harmonic of a Nd:YAG laser through objective O. The emission is collected with an immersion objective IO and sent either into an intensified CCD camera, with a flip mirror FM, or into a fiber leading to a time-multiplexed HBT detection setup. For spatial filtering, a confocal scheme including lenses L1 and L2 and removable pinhole P is used. Frequency filtering is performed with long-pass filter LF and bandpass filters F.

CdSe/CdS DRs with 2.7 nm core diameter, 22 nm shell length and 4 nm shell width. The DRs are dissolved in toluene with the concentration 10^{-14} mol/l^{-1} and coated onto a fused silica cover slip thus obtaining a surface density of less than 0.1 μm^{-2}.

In the experimental setup (figure 1), the excitation is with the pulsed third harmonic radiation of Nd:YAG laser with the wavelength 355 nm, pulse duration 18 ps and repetition rate 1 kHz. The energy per pulse can be varied with the help of a half-wave plate and a polarization beamsplitter; to reduce the probability of two-photon emission, it is chosen to be at 20% of the saturation level. In this case, a single DR manifests strong antibunching. For more than 10 single DRs we measured, the values of normalized CFs were below the upper boundaries determined by the measurement accuracy: $g_1^{(2)} \leqslant 0.05$, $g_1^{(3)} \leqslant 0.01$. A quarter-wave plate QWP transforms the polarization into circular, in order to provide the same excitation efficiency for all DRs regardless of their orientation. To uniformly excite many clusters of different sizes, the laser radiation is focused through an NA $= 0.65$ objective (O) placed on top of the sample, the illuminated area being 0.13 mm large. A fused silica cover slip with the DRs on top is placed over an NA $= 1.3$ oil immersion objective (IO). Because 86% of the DR emission is directed into the substrate [29] and the objective collects most of it, more than 70% of the emission is collected by the IO. Due to the use of thin fused silica cover slips the fluorescence noise is very low, leading to the signal-to-noise ratio higher than 3 even for the smallest cluster under study.

The DR emission is centered at 606 nm and has a full width at half maximum (FWHM) of 40 nm. A dichroic mirror reflects the pump and transmits the DR emission into the registration part of the setup. A long-pass filter (LF) with the cutoff wavelength 570 nm removes the remaining radiation of the pump. An intensified CCD (ICCD) camera (Princeton Instruments PI-MAX3:1024i) after a flip mirror (FM) is used to observe the image of several clusters and to choose ones containing different numbers of DRs. The image is formed by lens L with the focal distance 25 cm. As an example, figure 2(a) shows the images of several clusters. The radiation from the chosen cluster is selected by an iris aperture I and sent, by removing the FM M, through a multimode fiber into the Hanbury Brown–Twiss (HBT) setup using two avalanche photodiodes (APDs) and time multiplexing [30, 31]. (Note that, although the ICCD camera in single-photon regime can be used for the HBT measurement [8], its low quantum efficiency [32] does not allow detection of multiphoton events within a reasonable acquisition time.) The time multiplexing scheme contains a 60 m fiber loop (figure 1), so that each of the APDs can receive photons in one of the two time slots, separated by 300 ns. This scheme is then equivalent to a HBT setup with four detectors D1, D2, D3, D4, and enables the registration of up to four-fold coincidences and measurement of CFs of orders 2–4 [33]. To prevent cross-talk between the APDs, caused by flashes of light accompanying photon detections [34], 20 m of fiber is inserted in front of each APD.

For eliminating background noise (caused by stray light and fluorescence of the substrate and other optical elements), filters (F) are placed in front of both the ICCD and the HBT setup: another LF (cutoff wavelength 570 nm) and a bandpass filter (centered at 607 nm, with 42 nm FWHM). In addition, confocal microscopy

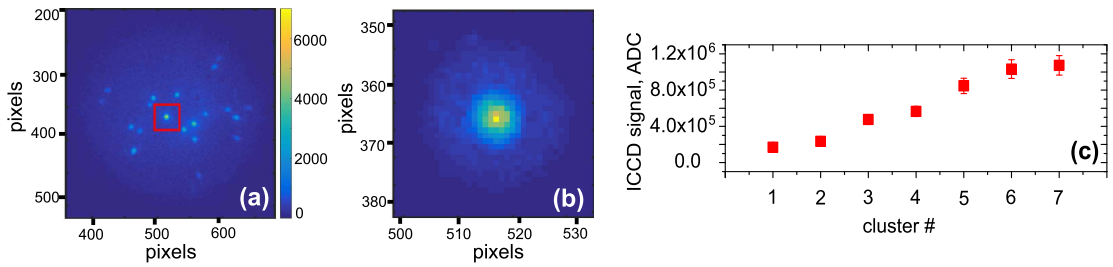

Figure 2. Several DR clusters imaged by the ICCD camera (a), the zoomed image of one of the clusters (red frame in panel a), selected with the confocal pinhole (b), and the integral signal from each cluster, with the noise subtracted (c).

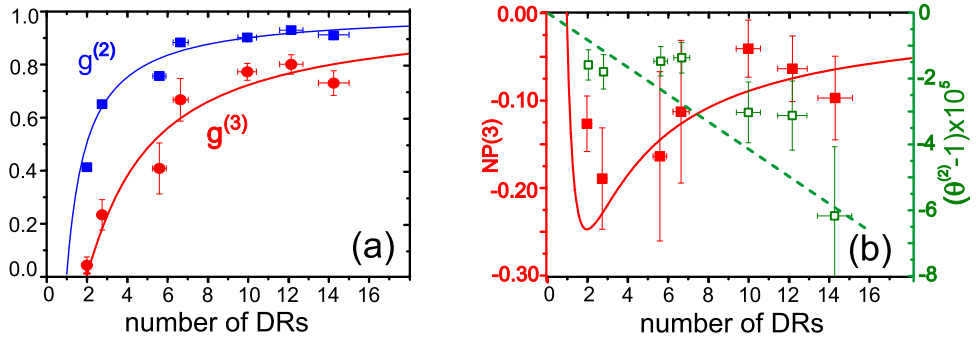

Figure 3. The second- (blue squares) and third-order (red circles) CFs (a) and the nonclassicality parameters NP(3) (red circles) and $\theta^{(2)} - 1$ (green squares) (b) measured for different clusters of DRs , versus the effective numbers m of DRs in these clusters.

filtering is arranged in front of the HBT setup by placing a 100 μm pinhole P between two confocal lenses (L1, L2) with focal lengths 7.5 cm. The image of a single cluster with the pinhole present is shown in figure 2(b).

4. Results and discussion

The data are taken for seven clusters, having different brightness in the ICCD image (figure 2(a)). After subtracting the background noise, the integral output signal obtained for these clusters varies from 1.7×10^5 to 1.1×10^6 analog-to-digital conversion units of the camera (figure 2(c)). As demonstrated in [8], this parameter can be used as an indicator of the number m of DRs in a cluster. This, together with the measured value $g^{(2)} = 0.413 \pm 0.009$ for the smallest cluster, allows us to conclude that the clusters contain from $m = 1.7 \pm 0.2$ to $m = 14 \pm 2$ DRs[7]. The mean number of photons per pulse detected from these clusters varies from 0.013 to 0.20. The low number of detected photons per pulse from a single DR (about 0.01) is due to the low excitation rate (10%) as well as the limited collection and detection efficiency.

For this reason, and because of the low rate of data acquisition (1 kHz), nearly no four-fold coincidences are acquired within several hours. Meanwhile, the number of detected two- and threefold coincidences suffices to measure the second- and third-order normalized CFs. This is done using the equation [35]

$$g^{(k)} = \frac{N_c^{(k)}}{N_1 \ldots N_k}, \tag{6}$$

where $N_c^{(k)}$ and N_i, $i = 1 \ldots k$, are the mean numbers of k-fold coincidences and photon counts in the ith detector, respectively, during a single pulse. Note that because of the low excitation and detection efficiency, $N_i \ll 1$, hence the probabilities to have a 'click' in the ith detector during a single pulse is $P_i \approx N_i \ll 1$, justifying the validity of equation (6) [14].

Figure 3(a) shows the normalized CFs measured for different clusters and plotted as functions of their size, estimated from their brightness. The lines show the theoretical fits with the relations for the normalized CFs of a group of m independent emitters. For the second-order CF of such a cluster, with the noise negligible, it is shown in appendix A that [8, 28]

[7] A fractional number of DRs means that different DRs can have different emission efficiencies.

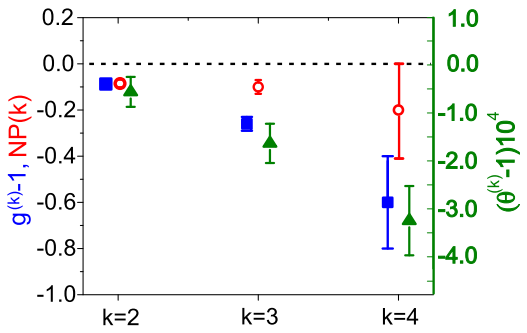

Figure 4. The second- to fourth-order nonclassical features measured for a cluster of 12 ± 1 DRs: NP(k) (red empty circles), $g^{(k)} - 1$ (blue filled squares) and $\theta^{(k)} - 1$ (green filled triangles) as functions of k. For better readability of the data, blue points are slightly shifted to the left and green points, to the right.

$$g_m^{(2)} = 1 + \frac{g_1^{(2)} - 1}{m}, \tag{7}$$

where $g_1^{(2)}$ is the normalized second-order CF of a single emitter. The third-order CF of such a cluster is calculated in appendix A to be

$$g_m^{(3)} = 1 + \frac{g_1^{(3)} + 3(m-1)g_1^{(2)} - 3m + 2}{m^2}, \tag{8}$$

where $g_1^{(3)}$ is the third-order normalized CF of a single emitter.

Theoretical dependences (solid lines in figure 3(a)) are plotted using (7) and (8) with $g_1^{(2)} = 0.01$ and $g_1^{(3)} = 0$[8]. The resulting curves are in a good agreement with the experimental points. All data points are below the unity, demonstrating antibunching of the second and third orders.

In figure 3(b), red points show the third-order nonclassicality parameter NP(3) for the same seven clusters, plotted versus their estimated size. One can see that it is negative for all clusters. This clearly indicates the nonclassicality; however, similarly to panel (a), the distance from the classical boundary decreases as the number of DRs in the cluster grows. This is shown by the theoretical dependence using expressions (7), (8) (solid line). Accordingly, the experimental results show a violation of the classical boundary by 3 standard deviations for small clusters and only 1–2 standard deviations for large ones.

The same panel shows the value of $\theta^{(2)} - 1$ (5), plotted with green empty squares. Here, unlike with the antibunching and NP(3), the distance from the classical boundary should increase with the increase in the size of the cluster. Indeed, we show in appendix B that if all emitters in a cluster have the same second-order CF, then

$$\theta^{(2)} - 1 = Cm(g_1^{(2)} - 1), \tag{9}$$

the parameter C scaling quadratically with the detection efficiency. This dependence is shown in figure 3(b) with the dashed green line. Deviations of the experimental points from this line are due to the difficulty to control the coupling of the emission into the fiber; the uncertainty in C reaches in this case 30%. Still, even for large clusters, violation of the classical inequality is about 3 standard deviations. Note that if some of the emitters in a cluster have $g_1^{(2)} > 1$, the dependence of $\theta^{(2)}$ on m can be different (see appendix B). The obtained monotonic dependence is an indication of the uniformity of the clusters.

Finally, for a chosen large cluster, containing 12 ± 1 DRs, during about 30 hours of acquisition we obtained a set of data with up to four-fold coincidences. These data enabled the measurement of the normalized CFs $g^{(k)}$ and the parameters NP(k).

The results are shown in figure 4. All three normalized CFs of orders 2–4 (blue filled squares) are well below the unity, demonstrating, for the first time to the best of our knowledge, up to the fourth-order antibunching. Meanwhile, the Klyshko nonclassicality parameters NP(k) (red empty circles) show negativity exceeding the measurement error only for $k = 2, 3$. Verification of nonclassicality for $k = 4$ requires more experimental data.

At the same time, condition $\theta^{(k)} - 1 < 1$ is satisfied for all $k = 2, 3, 4$, its violation growing with k. The reason is that in the limit of low detection probabilities P_i, expressions (5) for $k = 3, 4$ become (appendix B)

$$\theta^{(k)} - 1 \approx C\frac{k(k-1)}{2}m(g_1^{(2)} - 1), \tag{10}$$

[8] The curve looks the same for any $g_1^{(3)} \leqslant 0.05$.

the deviation from the classical boundary increases both with the number of emitters m and with the order k. Note that the latter tendency is the same for all nonclassicality parameters: the larger the order k, the larger the deviation from the classical boundary. At the same time, conditions $\theta^{(k)} < 1$ require less experimental data for verification than other conditions.

5. Conclusion

In conclusion, we have tested higher-order nonclassicality for clusters of 2–14 colloidal semiconductor DRs. Due to the use of both time-multiplexed APDs and an ICCD camera operating in single-photon regime, we were able to not only detect multiphoton events with relatively high efficiency, but also assess the number of DRs in a cluster. In addition to antibunching and its third- and fourth-order analogs, we have observed third-order Klyshko's nonclassicality, which has been shown to be a stronger condition. Note that the fourth-order antibunching and the third-order Klyshko nonlassicality, to the best of our knowledge, has been never observed before.

The low rate of detected single-photon emission (1% per excitation pulse) does not allow us to test higher-order antibunching or to witness fourth-order Klyshko nonclassicality. At the same time, for the nonclassicality parameters (5) it was possible to overcome the classical boundary up to the fourth-order, the deviation growing both with the order and with the size of the cluster.

The observed nonclassical features are important for QKD and quantum metrology, where nonclassical light with limited number of photons is required. Indeed, for light sources used in bipartite QKD, a small value of $g^{(2)}$ is required for the security against photon splitting attacks [36]; it means that an eavesdropper has little chance to get, simultaneously with the legitimate receiver, a photon carrying the information . Similarly, in multipartite QKD a group of n photons can be distributed between n legitimate receivers; whenever $g^{(n+1)} \ll 1$, the chance that an eavesdropper gets an additional photon carrying the information is small.

As to metrology, higher-order CFs are a measure of noise with respect to lower-order CFs. For instance, the simplest way to measure absorption is through intensity measurement. Then, the noise is determined by $g^{(2)}$ [37] and the accuracy is considerably increased by reducing it. But whenever the measurement is based on correlations, it is a higher-order CF that determines the accuracy. Reduction in this higher-order CF will considerably improve the measurement.

Possible QKD, metrology, or imaging protocols based on such multiphoton sources are still to be developed. But the observed nonclassical features are important prerequisites for these next steps.

Acknowledgments

The authors thank M Sondermann, V Salakhutdinov, and M Grassl for helpful discussions. LL and RF acknowledge the financial support of the Czech Science Foundation (GB14-36681G). LL acknowledges the financial support of Palacky University (IGA-PrF-2017-008).

Appendix A. CFs of a cluster of similar emitters

A cluster of incoherently emitting nanocrystals can be treated as a multimode source if the radiation of separate emitters is statistically independent. Here we derive the expressions for normalized CFs $g^{(k)}$ of different orders for such a cluster.

A.1. Second-order CF

Consider a cluster of m emitters generating photons incoherently. Assume that the emitters have the same value of second-order CF $g_1^{(2)}$ and the same mean number of emitted photons N_0. The total photon-number operator is the sum of the photon-number operators $\hat{N}_i$ for different emitters

$$\hat{N} = \sum_{i=1}^{m} \hat{N}_i, \ \langle \hat{N}_i \rangle = N_0. \tag{A.1}$$

The normalized second-order CF for the cluster will be

$$g^{(2)} = \frac{\langle :\hat{N}^2: \rangle}{\langle \hat{N} \rangle^2}, \tag{A.2}$$

where the dots denote normal ordering. We obtain

$$g^{(2)} = \frac{\langle :\left(\sum_{i=1}^{m}\hat{N}_i\right)^2:\rangle}{\langle\sum_{i=1}^{m}\hat{N}_i\rangle^2} = \frac{\sum_{i=1}^{m}\langle :\hat{N}_i^2:\rangle + \sum_{i\neq j}^{m}\langle\hat{N}_i\hat{N}_j\rangle}{(mN_0)^2}. \tag{A.3}$$

The first sum in the numerator contains m terms, each of them equal to $g_1^{(2)}N_0^2$. The second sum contains $m(m-1)$ terms equal to N_0^2 because $\langle\hat{N}_i\hat{N}_j\rangle = \langle\hat{N}_i\rangle\langle\hat{N}_j\rangle$. As a result, we get

$$g^{(2)} = 1 + \frac{g_1^{(2)} - 1}{m}, \tag{A.4}$$

which coincides with the expression for $g^{(2)}$ of light containing m modes with the same statistical properties [35].

Note that (A.4) can be extended to the case where the emitters have different mean photon numbers N_i, with m redefined as the 'effective' number of emitters

$$m_{eff} \equiv \frac{\left(\sum_{i=1}^{m}N_i\right)^2}{\sum_{i=1}^{m}N_i^2}. \tag{A.5}$$

This is in full analogy with the case of m independent modes with different mean photon numbers and the same CFs [38].

A.2. Third-order CF

The third-order CF for a cluster of m independent emitters with the same mean photon-number N_0 and third-order normalized CF $g_1^{(3)}$ is

$$g^{(3)} = \frac{\langle :\hat{N}^3:\rangle}{\langle\hat{N}\rangle^3}, \tag{A.6}$$

with $\hat{N}$ given by equation (A.1).

In this expression, the denominator is $m^3N_0^3$. For calculating the numerator, we will use the multinomial formula,

$$\left(\sum_{i=1}^{m}x_i\right)^k = \sum_{k_1+k_2+\ldots+k_m=k}\frac{m!}{k_1!k_2!\cdots k_m!}\prod_{t=1}^{m}x_t^{k_t}, \tag{A.7}$$

with $x_i = \hat{N}_i$ and $k = 3$.

We get

$$\langle :\hat{N}^3:\rangle = \sum_{i=1}^{m}\langle :\hat{N}_i^3:\rangle + 3\sum_{i\neq j=1}^{m}\langle :\hat{N}_i^2\hat{N}_j:\rangle + 6\sum_{i\neq j\neq k=1}^{m}\langle :\hat{N}_i\hat{N}_j\hat{N}_k:\rangle. \tag{A.8}$$

The first sum has m terms, each one equal to $g_1^{(3)}N_0^3$, the second one, $m(m-1)$ terms, each one equal to $g_1^{(2)}N_0^3$, and the third one, $m(m-1)(m-2)/6$ terms, each one equal to N_0^3. Then, the third-order normalized CF of the cluster is

$$g^{(3)} = 1 + \frac{g_1^{(3)} + 3(m-1)g_1^{(2)} - 3m + 2}{m^2}. \tag{A.9}$$

Dependences (A.4), (A.9) of the normalized second- and third-order CFs of a cluster on the number m of emitters are plotted in figure A1(a) by blue and red lines, respectively. Solid blue and dashed red lines denote the case of a cluster of ideal emitters ($g_1^{(2)} = g_1^{(3)} = 0$) and dotted blue and dashed–dotted red lines, the case of a cluster of nonideal identical emitters, $g_1^{(2)} = 0.2$, $g_1^{(3)} = 0.05$ [8, 14]. Note that all values of $g_1^{(3)} \leqslant 0.05$ lead to the curves that are indistinguishable in the figure. In both cases, $g^{(2)} < 1$ and $g^{(3)} < 1$ for any number of emitters in a cluster.

The third-order nonclassicality parameter, $\mathrm{NP}(3) = g^{(3)} - [g^{(2)}]^2$, is also negative for all m values (figure A1(b)), both in the ideal case (red solid line) and for $g_1^{(2)} = 0.2$, $g_1^{(3)} = 0.05$ (blue dashed line).

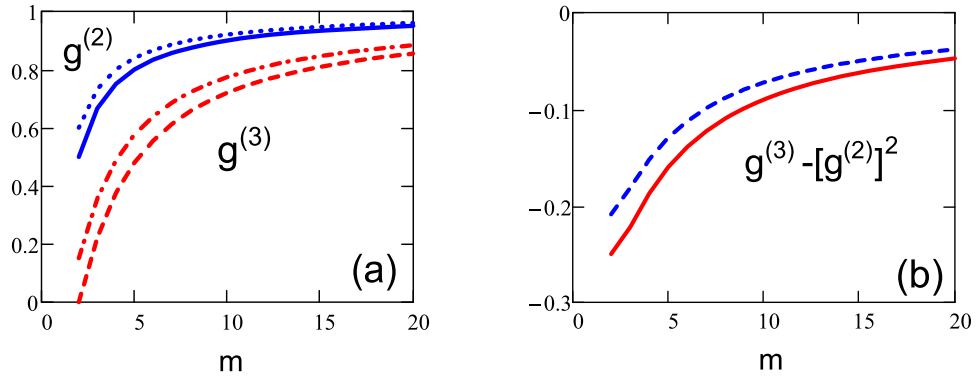

Figure A1. (a) Second-order (blue) and third-order (red) CF calculated for a cluster of ideal single-photon emitters (solid and dashed lines) and of nonideal emitters with $g_1^{(2)} = 0.2$, $g_1^{(3)} = 0.05$ (dash–dot and dotted lines) as functions of the number m of emitters; (b) the nonclassicality parameter for ideal (red solid line) and nonideal (blue dashed line) emitters versus their number m.

Appendix B. Nonclassicality parameters of orders 2–4 for a cluster

Let us now consider the nonclassicality parameters $\theta^{(k)}$ introduced in [18] for such a cluster. They are defined as

$$\theta^{(k)} = \frac{P_{0^{\otimes k}}}{\prod_{i=1}^{k} P_{0[i]}}, \tag{B.1}$$

where $P_{0^{\otimes k}}$ is the probability that neither of k detectors 'clicks' and $P_{0[i]}$ is the probability that the ith detector does not 'click'. As shown in [19]

$$\begin{aligned}
\theta_{ij}^{(2)} &= \frac{1 - P_i - P_j + P_{ij}}{(1 - P_i)(1 - P_j)}, \\
\theta_{ijk}^{(3)} &= \frac{1 - P_i - P_j - P_k + P_{ij} + P_{ik} + P_{jk} - P_{ijk}}{(1 - P_i)(1 - P_j)(1 - P_k)}, \\
\theta_{ijkl}^{(4)} &= \frac{1 - P_i - P_j - P_k - P_l + P_{ij} + P_{ik} + \ldots + P_{kl} - P_{ijk} - P_{ikl} - \cdots - P_{ljk} + P_{ijkl}}{(1 - P_i)(1 - P_j)(1 - P_k)(1 - P_l)},
\end{aligned} \tag{B.2}$$

where P_i is the probability that the ith detector clicks, P_{ij} is the probability that both detectors i, j click, and so on.

Because in our experiments, similarly to many experiments with single-photon emitters, the click probabilities are very small,

$$P_i \ll 1, \tag{B.3}$$

one can write

$$\begin{aligned}
P_{ij} &= g^{(2)} P_i P_j, \\
P_{ijk} &= g^{(3)} P_i P_j P_k, \\
P_{ijkl} &= g^{(4)} P_i P_j P_k P_l.
\end{aligned} \tag{B.4}$$

As a result, it follows from (B.5) that

$$\begin{aligned}
1 - \theta_{ij}^{(2)} &= \frac{(1 - g^{(2)}) P_i P_j}{(1 - P_i)(1 - P_j)}, \\
1 - \theta_{ijk}^{(3)} &= \frac{(1 - g^{(2)})(P_i P_j + P_i P_k + P_j P_k) - (1 - g^{(3)}) P_i P_j P_k}{(1 - P_i)(1 - P_j)(1 - P_k)}, \\
1 - \theta_{ijkl}^{(4)} &= [(1 - g^{(2)})(P_i P_j + \ldots + P_k P_l) - (1 - g^{(3)})(P_i P_j P_k + \ldots + P_j P_k P_l) \\
&\quad + (1 - g^{(4)}) P_i P_j P_k P_l] / [(1 - P_i)(1 - P_j)(1 - P_k)(1 - P_l)].
\end{aligned} \tag{B.5}$$

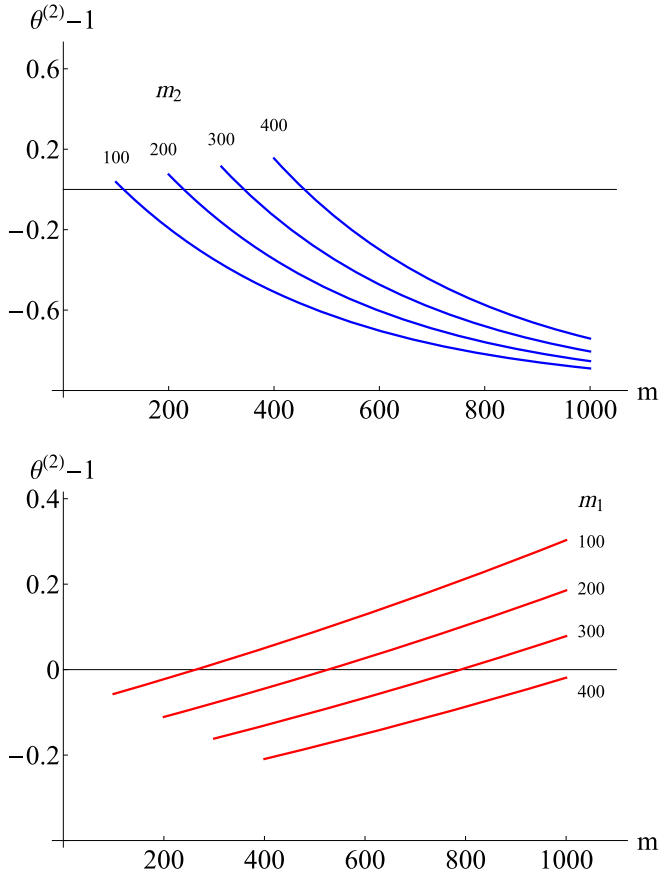

Figure B1. The effect of the cluster size on the parameter $\theta^{(2)} - 1$. The cluster consists of m_1 emitters with $g^{(2)} = 0.4$ and m_2 emitters with $g^{(2)} = 1.6$. The total number of emitters (horizontal axis) is $m = m_1 + m_2$. Top: fixed $m_2 = 100, 200, 300, 400$ and increasing m_1 result in the decrease of $\theta^{(2)}$. Bottom: fixed $m_1 = 100, 200, 300, 400$ and increasing m_2 lead to the growth of $\theta^{(2)}$.

Under condition (B.3)

$$\begin{aligned} 1 - \theta^{(2)}_{ij} &\approx (1 - g^{(2)}) P_i P_j, \\ 1 - \theta^{(3)}_{ijk} &\approx (1 - g^{(2)})(P_i P_j + P_i P_k + P_j P_k) = 3\overline{(1 - \theta^{(2)}_{ij})}, \\ 1 - \theta^{(4)}_{ijkl} &\approx (1 - g^{(2)})(P_i P_j + \ldots + P_k P_l) = 6\overline{(1 - \theta^{(2)}_{ij})}, \end{aligned} \tag{B.6}$$

where the horizontal line denotes averaging over all combinations of detector pairs.

In the general case, the emitters forming a cluster can have different properties like, for instance, different $g^{(2)}$ values. While the CFs of different orders always tend to the unity as the number m of emitters increases, the situation is different for the $\theta^{(k)}$ nonclassicality parameters. As an example, figure B1 shows the parameter $\theta^{(2)} - 1$ simulated for clusters containing a large number of emitters with different values of $g^{(2)}$. In the first case, the size of the cluster increases by adding emitters with $g^{(2)} < 1$ and in the second case, emitters with $g^{(2)} > 1$. One can see that these two cases affect the resulting $\theta^{(2)} - 1$ differently: in the first case, the parameter drops and the nonclassicality gets more visible, while in the second case, $\theta^{(2)}$ grows and the nonclassicality disappears after a certain m.

Two conclusions are important for the data analysis in the main text.

1. Because the detection probability scales as the detection efficiency η times the number of emitters in the cluster, $P_i \propto \eta m$, and, according to equation (A.4), $1 - g^{(2)} = (1 - g_1^{(2)})/m$, it follows that

$$1 - \theta^{(2)}_{ij} = Cm(1 - g_1^{(2)}), \tag{B.7}$$

where C depends quadratically on the detection efficiency η. Thus, the second-order nonclassicality gets more pronounced as the number of emitters grows.

2. Due to equation (B.6) and their obvious extrapolation to higher orders, under low detection probabilities, and provided that an averaging is performed over all detector combinations, nonclassicality parameters of all orders are proportional to the second-order one,

$$1 - \theta^{(k)}_{i_1 \ldots i_k} = \frac{k(k-1)}{2}\overline{(1 - \theta^{(2)}_{ij})}. \tag{B.8}$$

ORCID iDs

Luigi Carbone https://orcid.org/0000-0002-1369-6890

References

[1] Braunstein S L and McLachlan R I 1987 Generalized squeezing *Phys. Rev.* A **35** 1659
[2] Douady J and Boulanger B 2004 Experimental demonstration of a pure third-order optical parametric downconversion process *Opt. Lett.* **29** 2794
[3] Moebius M G, Herrera F, Griesse-Nascimento S, Reshef O, Evans C C, Guerreschi G G, Aspuru-Guzik A and Mazur E 2016 Efficient photon triplet generation in integrated nanophotonic waveguides *Opt. Express* **39** 9932
[4] Cavanna A, Just F, Jiang X, Leuchs G, Chekhova M V, Russell P St J and Joly N Y 2016 Hybrid photonic-crystal fiber for single-mode phase matched generation of third harmonic and photon triplets *Optica* **3** 952
[5] Khoshnegar M *et al* 2016 A solid state source of photon triplets based on quantum dot molecules *Nat. Commun.* **8** 15716
[6] Wang X-L *et al* 2016 Experimental ten-photon entanglement *Phys. Rev. Lett.* **117** 210502
[7] Harder G, Bartley T J, Lita A E, Nam S W, Gerrits T and Silberhorn C 2016 Single-mode parametric-down-conversion states with 50 photons as a source for mesoscopic quantum optics *Phys. Rev. Lett.* **116** 143601
[8] Shcherbina O A, Shcherbina G A, Manceau M, Vezzoli S, Carbone L, De Vittorio M, Bramati A, Giacobino E, Chekhova M V and Leuchs G 2014 Photon correlations for colloidal nanocrystals and their clusters *Opt. Lett.* **39** 1791
[9] Scarani V, Bechmann-Pasquinucci H, Cerf N J, Dušek M, Lütkenhaus N and Peev M 2009 The security of practical quantum key distribution *Rev. Mod. Phys.* **81** 1301
[10] Giovannetti V, Lloyd S and Maccone L 2011 Advances in quantum metrology *Nat. Photon.* **5** 222
[11] Straka I, Lachman L, Hlousek J, Mikova M, Micuda M, Jezek M and Filip R 2018 Quantum non-gaussian multiphoton light *NPJ Quant. Inf.* **4** 4
[12] Leonhardt U 1997 *Measuring the Quantum state of Light* (Cambridge: Cambridge University Press)
[13] Klyshko D N 1996 The nonclassical light *Phys.—Usp.* **39** 573
[14] Stevens M J, Glancy S, Nam S W and Mirin R P 2013 Third-order antibunching from an imperfect single-photon source *Opt. Exp.* **22** 3244
[15] Rundquist A, Bajcsy M, Majumdar A, Sarmiento T, Fischer K, Lagoudakis K G, Buckley S, Piggott A Y and Vuckovic J 2014 Nonclassical higher-order photon correlations with a quantum dot strongly coupled to a photonic-crystal nanocavity *Phys. Rev.* A **90** 023846
[16] Sperling J, Vogel W and Agarwal G S 2013 Correlation measurements with on-off detectors *Phys. Rev.* A **88** 043821
[17] Filip R and Lachman L 2013 Hierarchy of feasible nonclassicality criteria for sources of photons *Phys. Rev.* A **88** 043827
[18] Lachman L, Slodicka L and Filip R 2015 Nonclassical light from a large number of independent single-photon emitters *Sci. Rep.* **6** 19760
[19] Moreva E, Traina P, Forneris J, Degiovanni I P, Ditalia Tchernij S, Picollo F, Brida G, Olivero P and Genovese M 2017 Direct experimental observation of nonclassicality in ensembles of single-photon emitters *Phys. Rev.* B **96** 195209
[20] Obsil P, Lachman L, Pham T, Lesundak A, Hucl V, Czek M, Hrabina J, Cip O, Slodicka L and Filip R 2017 Nonclassical light from large ensemble of trapped ions arXiv:1705.04472 [quant-ph]
[21] Michler P, Imamoglu A, Mason M D, Carson P J, Strouse G F and Buratto S K 2000 Quantum correlation among photons from a single quantum dot at room temperature *Nature* **406** 968
[22] Efros A and Rosen M 1997 Random telegraph signal in the photoluminescence intensity of a single quantum dot *Phys. Rev. Lett.* **78** 1110
[23] van Sark W G J H M, Frederix P L T M, Van den Heuvel D J and Gerritsen H C 2001 Photooxidation and photobleaching of single CdSe/ZnS quantum dots probed by room-temperature time-resolved spectroscopy *J. Phys. Chem.* B **105** 8281
[24] Carbone L *et al* 2007 Synthesis and micrometer-scale assembly of colloidal cdse/cds nanorods prepared by a seeded growth approach *Nano Lett.* **7** 2942
[25] Pisanello F *et al* 2010 Room temperature-dipolelike single photon source with a colloidal dot-in-rod *Appl. Phys. Lett.* **96** 033101
[26] Manceau M, Vezzoli S, Glorieux Q, Pisanello F, Giacobino E, Carbone L, De Vittorio M and Bramati A 2014 Effect of charging on CdSe/CdS dot-in-rods single-photon emission *Phys. Rev.* B **90** 035311
[27] Vezzoli S, Manceau M, Lemenager G, Glorieux Q, Giacobino E, Carbone L, De Vittorio M and Bramati A 2015 Exciton fine structure of CdSe/CdS nanocrystals determined by polarization microscopy at room temperature *ACS Nano* **9** 7992
[28] Israel Y, Tenne R, Oron D and Silberberg Y 2017 Quantum correlation enhanced super-resolution localization microscopy enabled by a fibre bundle camera *Nat. Commun.* **8** 14786
[29] Lukosz W 1979 Light emission by magnetic and electric dipoles close to a plane dielectric interface: III. Radiation patterns of dipoles with arbitrary orientation *J. Opt. Soc. Am.* **69** 1495
[30] Achilles D, Silberhorn C, Sliwa C, Banaszek K and Walmsley I A 2003 Fiber- assisted detection with photon number resolution *Opt. Lett.* **28** 2387
[31] Fitch M J, Jacobs B C, Pittman T B and Franson J D 2003 Photon-number resolution using time-multiplexed single-photon detectors *Phys. Rev.* A **68** 043814
[32] Qi L, Just F, Leuchs G and Chekhova M V 2016 Autonomous absolute calibration of an ICCD camera in single-photon detection regime *Opt. Express* **24** 26444

[33] Avenhaus M, Laiho K, Chekhova M V and Silberhorn C 2010 Accessing higher order correlations in quantum optical states by time multiplexing *Phys. Rev. Lett.* **104** 063602
[34] Kurtsiefer C, Zarda P, Mayer S and Weinfurter H 2001 The breakdown flash of silicon avalanche photodiodes-back door for eavesdropper attacks? *J. Mod. Opt.* **48** 2039
[35] Ivanova O A, Iskhakov T Sh, Penin A N and Chekhova M V 2006 Multiphoton correlations in parametric down-conversion and their measurement in the pulsed regime *Quantum Electron.* **36** 951
[36] Waks E, Santori C and Yamamoto Y 2002 Security aspects of quantum key distribution with sub-Poisson light *Phys. Rev.* A **66** 042315
[37] Moreau P-A, Sabines-Chesterking J, Whittaker R, Joshi S K, Birchall P M, McMillan A, Rarity J G and Matthews J C F 2016 Demonstrating an absolute quantum advantage in direct absorption measurement *Sci. Rep.* **7** 6256
[38] Finger M A, Iskhakov T Sh, Joly N Y, Chekhova M V and Russell P St J 2015 Raman-free, noble-gas-filled PCF source for ultrafast, very bright twin-beam squeezed vacuum *Phys. Rev. Lett.* **115** 143602